IOP Publishing Journal of Neural Engineering
J. Neural Eng. 13 (2016) 036022 (17pp) doi:10.1088/1741-2560/13/3/036022

A simple method for EEG guided transcranial electrical stimulation without models

Andrea Cancelli[1,2], Carlo Cottone[1], Franca Tecchio[1], Dennis Q Truong[3], Jacek Dmochowski[3] and Marom Bikson[3]

[1] Laboratory of Electrophysiology for Translational neuroScience (LET'S)—ISTC—CNR, Italy
[2] Institute of Neurology, Catholic University, Rome, Italy
[3] Department of Biomedical Engineering, The City College of New York, New York, NY 10031, USA

E-mail: andrea.cancelli86@gmail.com

Received 15 December 2015, revised 8 April 2016
Accepted for publication 22 April 2016
Published 11 May 2016

Abstract

Objective. There is longstanding interest in using EEG measurements to inform transcranial Electrical Stimulation (tES) but adoption is lacking because users need a simple and adaptable recipe. The conventional approach is to use anatomical head-models for both source localization (the EEG inverse problem) and current flow modeling (the tES forward model), but this approach is computationally demanding, requires an anatomical MRI, and strict assumptions about the target brain regions. We evaluate techniques whereby tES dose is derived from EEG without the need for an anatomical head model, target assumptions, difficult case-by-case conjecture, or many stimulation electrodes. *Approach.* We developed a simple two-step approach to EEG-guided tES that based on the topography of the EEG: (1) selects locations to be used for stimulation; (2) determines current applied to each electrode. Each step is performed based solely on the EEG with no need for head models or source localization. Cortical dipoles represent idealized brain targets. EEG-guided tES strategies are verified using a finite element method simulation of the EEG generated by a dipole, oriented either tangential or radial to the scalp surface, and then simulating the tES-generated electric field produced by each model-free technique. These model-free approaches are compared to a 'gold standard' numerically optimized dose of tES that assumes perfect understanding of the dipole location and head anatomy. We vary the number of electrodes from a few to over three hundred, with focality or intensity as optimization criterion. *Main results.* Model-free approaches evaluated include (1) voltage-to-voltage, (2) voltage-to-current; (3) Laplacian; and two Ad-Hoc techniques (4) dipole sink-to-sink; and (5) sink to concentric. Our results demonstrate that simple ad hoc approaches can achieve reasonable targeting for the case of a cortical dipole, remarkably with only 2–8 electrodes and no need for a model of the head. *Significance.* Our approach is verified directly only for a theoretically localized source, but may be potentially applied to an arbitrary EEG topography. For its simplicity and linearity, our recipe for model-free EEG guided tES lends itself to broad adoption and can be applied to static (tDCS), time-variant (e.g., tACS, tRNS, tPCS), or closed-loop tES.

Keywords: EEG, computational modeling, tES, evoked potentials, MRI, reciprocity

(Some figures may appear in colour only in the online journal)

Introduction

The idea of using EEG recordings to optimize transcranial Electrical Stimulation (tES) configuration has been discussed for decades [1]. The conceptual appeal is evident: owing to the apparent symmetry of the transfer function between brain and scalp space, the EEG measurements represents task/subject specific brain activity as detected at the scalp, which

in principle should reflect task/subject specific brain regions to be targeted by tES. The relationship between scalp EEG and tES is formalized by the reciprocity principle: the electrical path taken by an applied scalp current to the location of a biological current source, is symmetric to the path taken by the activation of that biological source to the (now recording) scalp electrodes (Helmholtz, 1853; Rush and Driscoll, 1969). But this theoretical principle does not directly inform a method for practical implementation. A 'brute force' implementation using numerical simulations of tES targeting requires anatomically specific models (subject specific scans and tissue segmentation; [2, 3]), statistical assumptions for source localization from EEG that have yet to be validated [4], and computationally intensive dose optimization for tES [5, 6]. Moreover, this workflow is subject to a hard decision (i.e., commitment to the implicated brain region) on target selection and how to quantify a 'good' optimization result [5]. Thus, despite highly compelling value for EEG-guided tES (see below), adoption is limited by methods that are burdensome and/or poorly constrained [1, 7, 8].

Typically when, without a model, EEG is used to identify a target [9–11] or to select tES waveform [11–13], electrodes (often large pads) are positioned based on rules-of-thumb such as placing one electrode 'over' the region of interest and the other one at 'some distance'. Model-driven efforts on EEG guided tES have been considered with increasing sophistication and computational burden [7, 14, 15]. tES-EEG 'reciprocity' is a concept adapted from the circuit theory and requires a head model (circuit path) to specify reciprocity between each electrode and brain region [8, 16, 17].

Though a longstanding notion, recent developments make EEG guided tES more desirable and feasible. For example, despite encouraging results from human trials of tES [18–23], there are concerns about inter- and intra-individual variability [24–27]. So a need exists for methods to customize dose, ideally in a manner that is not burdensome (e.g., not neuro-navigated). Indeed, clinically effective (FDA-approved) neuromodulation technology typically requires patient-specific setup for success, including neuronavigated TMS and DBS [28–31]; clinical adoption of tES may ultimately be supported through EEG-guidance. EEG-informed tES can be implemented under open-loop, where EEG is imaged before stimulation [32], or as closed-loop regimes given that scalp EEG patterns vary in time, and tES has been shown to modulate EEG activity [33–37]. EEG-guided tES is supported by increased sophistication in EEG and stimulation hardware [14, 15, 38]. For example, compact gel-based electrodes designed for tES (high-definition electrodes; [39, 40]) allow integration with EEG headgear (e.g., HD-tDCS, HD-tACS; [41–45]) including the reproduction of conventional pad montages [46]. What is lacking is a simple recipe for mapping EEG measurements into tES parameters.

The ideal methodological approach would: (1) not require subject specific imaging (not neuro-navigated [47]; (2) automatically adapt to any EEG electrode deployment (e.g., 10-10, concentric, custom) and inject current through the same electrodes (positions); while (3) limiting the number of electrodes used for tES, regardless of EEG density, to a selectable amount (balancing reasons to minimize stimulation channels with current per electrode); (4) account for neural source orientation as well as position [48]; while (5) naturally balancing tES optimization for focality versus intensity, which can be divergent criteria [5]; (6) be linear or otherwise apply to any static (tDCS) or time-dependent application (tACS); while (7) lending itself to various forms of EEG analysis (e.g., filtering) and decomposition [38]; (8) allow specific current limits based on tolerability and safety standards (e.g., maximum current per channel [49–51]); but notwithstanding all the above (9) remain computationally light, allowing even closed-loop applications (e.g., a dynamic EEG and tES). An approach fulfilling these criteria would be simple and broadly deployable, and thus facilitate diverse applications of EEG-guided tES—essentially in any domain where there is an EEG marker of the cognitive/behavioral target with inter-individual variability [52–57]. The model-free techniques evaluated here, and particularly the proposed approaches that select a limited number of electrodes for stimulation based on EEG features, aim to achieve these goals.

Methods

Finite element model

An exemplary [25, 58, 59] MRI-derived finite element model of a head of a subject who reported no cerebral damage was generated from a 3T MRI scan that had an isotropic 1 mm^3 resolution. The MRI was segmented by ScanIP software (Simpleware, Exeter, UK) which each voxel isotropic conductor volume assigned one of seven conductivities [60–68]: air (10^{-15} S m^{-1}), bone (10^{-2} S m^{-1}), cerebrospinal fluid (CSF, 1.65 S m^{-1}), fat (0.025 S m^{-1}), gray matter (0.276 S m^{-1}), skin (0.465 S m^{-1}), white matter (0.126 S m^{-1}). Dipoles are often used as representations for electrically-active patches of neuronal tissue [69–72]. We separately modeled two dipoles, one tangential and one radial to the cortex. Each dipole source was simulated by 2 voxels, negative and positive poles, separated by 1 mm. Dipoles were positioned on the left hemisphere of the somatosensory cortex, in the Brodmann area 3 over the somatotopic representation of the hand. The two dipoles patterned the cortical activation of a sensory evoked potential generated by the right median nerve stimulation [73–75].

331 high definition (HD) electrodes (disc electrodes having skin contact area of 0.8 cm^2 each) with realistic underlying gel (0.3 S m^{-1}) were projected onto the scalp surface as tissue segmentations using a previously developed Matlab script (Kempe *et al* 2014) [15, 25, 38, 46, 48, 58–76]. Electrodes were distributed across the scalp surface of the model (figures 1(A) and (B)) allocated according to the International 10-10 System [77] and 10-5 submultiples. It included two axial lines of electrodes below the plane of the eyes, and one electrode over the back of the neck (which was used as a reference), except avoiding regions over the orbit, ears, and nose. The scalp electrodes were used to either to (1) simulate EEG by collecting voltage over the scalp produced by brain dipoles, or (2) deliver current during tES with a set current at each electrode.

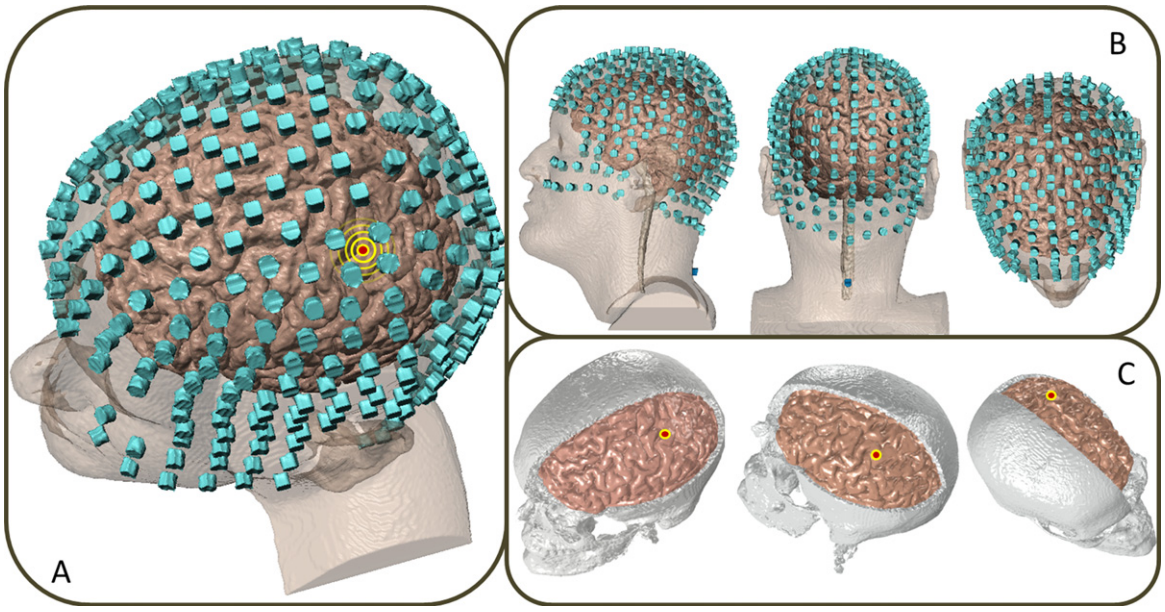

Figure 1. Source and electrodes. (A) Wide angle 3D view of the subject's head showing the full set of recording/stimulating scalp electrodes used for the EEG-to-tES mapping (cyan color) and the stereotaxic position of the source inserted into the cortex (red and yellow). (B) Full set of scalp electrodes in sagittal, coronal and axial view. (C) Other views of the source inserted into the brain to mimic a hand sensory evoked potential (SEP): left cerebrum, frontal lobe, postcentral gyrus, gray matter, Brodmann area 3.

Adaptive volumetric meshing was applied to the tissue segmentation in ScanIP (Simpleware Ltd, Exeter, UK) with a compound coarseness of −15 (maximum edge length 1.85 mm, target minimum 0.775 mm, target Jacobian minimum 0.1). The resulting meshes consisted of >10 000 000 quadratic tetrahedral elements and >15 million degrees of freedom. Further refined meshes were found to have no noticeable effect on simulation results. The mesh was imported in COMSOL Multiphysics 4.3 (Burlington, MA) to simulate quasi-static volume conductor physics. The quasi-static approximation is considered reasonable for both EEG and tES [67, 78–81]. Within COMSOL, the Laplace equation ($\nabla \cdot (\sigma \nabla V) = 0$, $\nabla \cdot$: divergence; ∇ : gradient; σ : conductivity; V : electric potential) was solved for voltage distribution given distinct Dirichlet or Neumann boundary conditions depending on EEG or tES simulation. COMSOL implemented a linear system solver of conjugate gradients with a relative tolerance of 1×10^{-6}.

tES simulation: electrode activation

When current stimulation was applied in the tES condition, a boundary condition of normal current density was implemented to each stimulating electrode. For each electrode, the current value was divided by the skin-electrode contact area and was applied as current density boundary condition and assigned to the mesh nodes as current loads representing the right-hand-side of the linear system of equations.

EEG simulation: brain source activations

An electric potential of 1 mV, with boundary conditions −0.5 mV at the negative pole and +0.5 mV at the positive one, was applied to the brain sources for each dipole direction. The positive pole was chosen to point towards the frontal lobe for the tangentially-oriented dipole, and the positive pole toward the scalp surface for the radially-oriented dipole. For the EEG simulation, to obtain a correct scalp voltage distribution, the conductivity of the HD electrodes over the scalp surface was set $\sigma = 10^{-9}$ (e.g., analogous to electrodes connected to a high impedance EEG amplifier). The computed voltage was sampled from the electrode center. Such value, because of the small electrode size, showed, indeed, negligible difference with the averaged voltage under the electrode's surface. We simulated the EEG potentials from 330 electrodes with the neck electrode being the reference [82]. The dipole models produced two different characteristic scalp voltage distributions ([73–75]; figure 2, top).

In some cases, voltage only sub-multiples or Ad-Hoc electrodes were used to determine tES dose (see *electrode montage selection*).

Model-free approaches

The central objective of this paper is to evaluate various approaches for tES based on EEG without the dependence on a head model. A head model was however employed to emulate an exemplary EEG and to verify the performance of these approaches only in the evaluation of this paper. We emphasize that the steps that generate the information guiding tES are model-free. For our model-free processes (table 1) we distinguish between two methods: (A) EEG-to-tES mapping techniques, where the voltage or current applied to each tES electrode is determined; and (B) electrode montage selection, where the number and location of electrodes used for tES is determined—sampled from the electrodes used for EEG. The

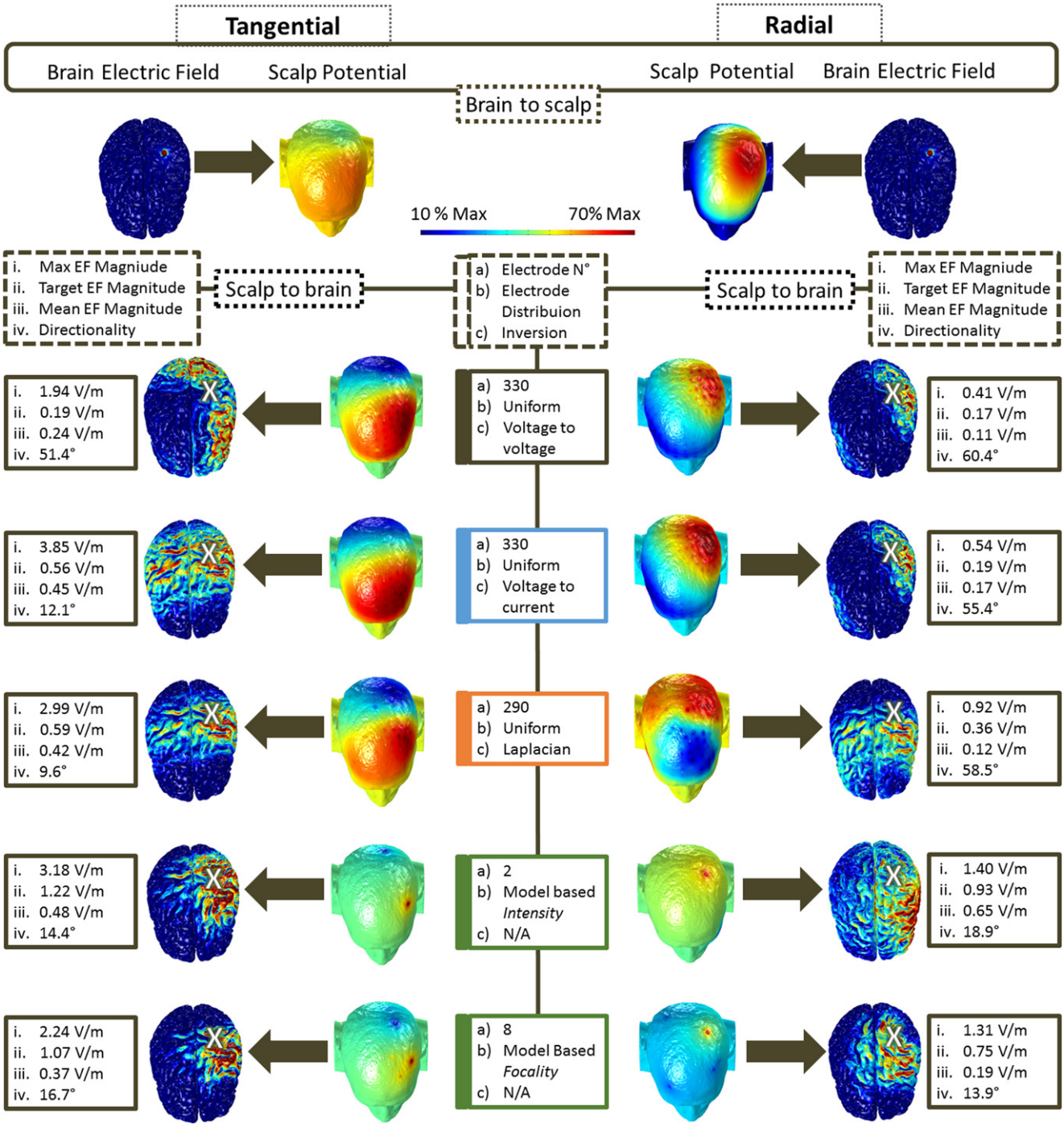

Figure 2. Different EEG-to-tES mappings using the maximum number of stimulating electrodes. First row: sensory cortex source producing an electric field from the brain to the scalp in two different directions, tangential and radial to the cortex trough two electric charges generating 1 mV. The scalp potential distribution generated by the source was simulated by 330 electrodes. Second to fourth row. The scalp potential simulated in the two direction was used to apply three different montages performing tDCS stimulations. The EEG values were applied as voltage (second row), current (third row) and current after calculating the Laplacian at all channels. Fifth and sixth row. Two model-based optimized montages, one for intensity and one for focality.

EEG-to-tES mapping technique is thus only applied to the set of tES electrodes selected.

EEG-to-tES mapping technique. This section addresses assignment of stimulation voltage or current to the pre-selected electrodes for five model-free approaches. In three approaches the current applied is calculated from the simulated EEG: 'voltage-to-voltage', 'voltage-to-current', and 'Laplacian'. For these approaches either uniform or Ad-Hoc tES electrode selection (see 'tES electrode montage selection' paragraph) can be applied. For the remaining two approaches 'sink-to-sink' and 'sink-to-concentric ring', the current values applied were not

Table 1. Electrode montages. For each montage, different types of EEG-to-tES mapping techniques were tested.

Dipole direction	Electrode distribution		Inversion technique	Electrode number
Tangential	Uniform		Voltage to Voltage	330
			Voltage to Current	330,256, 128, 64, 32, 16, 8
			Laplacian	290,256, 128, 64, 32, 16, 8
	Ad Hoc	Voltage	Voltage to Current	8 (4 X 4), 4 (2 X 2)
			Sink to Sink	2 (1 X 1)
		Laplacian	Laplacian	8 (4 X 4), 4 (2 X 2)
			Sink to Sink	2 (1 X 1)
	Model Based		N/A	8 (4 X 4), 2 (1 X 1)
Radial	Uniform		Voltage to Voltage	330
			Voltage to Current	330
			Laplacian	290
	Ad Hoc	Voltage	Sink to Concentric Ring	5 (4 X 1), 6 (4 X 2),6 (5 X 1)
		Laplacian	Laplacian	8 (4 X 4), 4 (2 X 2)
			Sink to Sink	2 (1X1)
	Model Based		N/A	8 (4 X 4), 2 (1 X 1)

calculated from the EEG information, but electrode selection was EEG guided using the Ad-Hoc tES electrode selection.

Voltage-to-voltage. This is a basic EEG-to-tES mapping technique in which the voltage EEG values are applied to the stimulating electrodes.

For each channel:

$$\Delta V_1^{\text{stim}} = -\frac{\Delta V_1^{\text{EEG}}}{\Delta V_{\text{tot}}^{\text{EEG}}} \cdot \Delta V,$$
$$\Delta V_n^{\text{stim}} = -\frac{\Delta V_n^{\text{EEG}}}{\Delta V_{\text{tot}}^{\text{EEG}}} \cdot \Delta V.$$

To apply a zero average stimulation of 1 mV, the potential of each electrode (ΔV_i^{stim}) was divided by the sum of all the potentials with the same polarity ($\Delta V_{\text{tot}}^{\text{EEG}}$) and then multiplied by $\Delta V = 0.5$ mV. Uniform and Ad-Hoc positioning were applied.

Voltage-to-current. The zero average referenced values (see voltage-to-voltage section) were applied to the electrodes as current

$$I_1^{\text{stim}} = -\frac{\Delta V_1^{\text{EEG}}}{\Delta V_{\text{tot}}^{\text{EEG}}} \cdot I,$$
$$I_n^{\text{stim}} = -\frac{\Delta V_n^{\text{EEG}}}{\Delta V_{\text{tot}}^{\text{EEG}}} \cdot I,$$

where I_i^{stim} is the current intensity applied at each electrode and I is the total current delivered through all the electrodes. In all the simulations total current was set $I = 1$ mA (+1 mA of total anodic and −1 mA of cathodic current intensity). Uniform and Ad-Hoc positioning were applied.

Laplacian. The Laplacian operator was applied to the EEG values. Surround electrodes were defined as those centered within a 3 cm radius of the evaluated electrode channel. In this way, we obtained a complete ring of electrodes around each channel to estimate the average to subtract. In the case that one electrode was not circumscribed by a complete ring of electrodes, it was excluded from the stimulation. Potentially, for the Laplacian montage, if information about the cortical region involved in the source activation is known, as it is during an evoked potential EEG, a different weight among the channels can be applied to increase the focality of

the Laplacian *EEG-to-tES mapping technique*

$$I_1^{\text{stim}} = -\frac{\left(\Delta V_1^{\text{EEG}} - \sum_{i=1}^{z} \frac{w_i \cdot \Delta V_i^{\text{EEG}}}{n}\right)}{\Delta V_{\text{tot}}^{\text{EEG}}} \cdot I,$$

$$I_n^{\text{stim}} = -\frac{\left(\Delta V_n^{\text{EEG}} - \sum_{i=1}^{z} \frac{w_i \cdot \Delta V_i^{\text{EEG}}}{n}\right)}{\Delta V_{\text{tot}}^{\text{EEG}}} \cdot I.$$

The weight w was set as a unitary vector for all the channels to not introduce difference in evaluating the different approaches.

The obtained values were zero averaged and normalized to deliver 1 mA of total current intensity for all the selected montages. Uniform and Ad-Hoc positioning were applied.

Sink-to-sink. This is a 1 × 1 configuration, having one anode and one cathode. The boundary condition of 1 mA was set for the anode, while the cathode was set as ground (effectively collecting −1 mA).

Sink-to-ring. Concentric ring electrode configurations were applied using 1 mA for the central cathodes and setting the anodes as ground.

tES Electrode montage selection. The EEG-to-tES mapping approaches evaluated in this work were applied using two general approaches to select number and location of tES electrodes: those based on uniform distribution and those based on EEG guided Ad-Hoc selection (table 1).

Uniform. In this case either the entire set of 330 electrodes is used, which were distributed using the International Systems EEG positioning (see above) or uniform sub-multiples: 256, 128, 64, 32, 16, 8 electrodes. Uniform selection is independent of the EEG generated. The current applied to each electrode in the uninform set is always based on the EEG (see EEG-to-tES mapping techniques) but we emphasize that the selection of electrodes for the uniform case is not based on the EEG.

Ad-Hoc. This electrode selection is based on specific EEG topographies. Two general approaches are used to select tES electrodes based on the EEG: either electrodes are selected by maximum/minimum EEG voltage or maximum/minimum EEG Laplacian. While the EEG voltage and Laplacian are calculated as described in the sections above, it is important to distinguish between the use of this information to select electrodes in this section, with the subsequent use of this information to determine applied current at selected electrodes. The methods for selecting number of electrodes based on Ad-Hoc approaches available for tES are described below and vary from 2 to 8. For the different Ad-Hoc techniques, the current applied at each electrode may or may not be calculated from the EEG, depending on the approach:

- 1 × 1 (2 electrodes), one anode and one cathode were selected as the EEG electrodes with minimum and maximum (bipolar distribution case) voltages (Ad-Hoc voltage) or Laplacian (Ad-Hoc Laplacian). The sink-to-sink mapping technique was applied to this montage, which reproduces a bipolar distribution and where the applied current does not depend on the EEG.
- 2 × 2 (4 electrodes) two anodes and two cathodes were selected as the EEG electrodes with the two minimum and maximum values (bipolar distribution case) of voltage (Ad-Hoc Voltage) or Laplacian (Ad-Hoc Laplacian). The Voltage-to-Current and Laplacian approaches were applied to this montage, which reproduces a bipolar distribution and where the applied current depend on the EEG.
- 4 × 4 (8 electrodes) four anodes and four cathodes were selected as the EEG electrodes with the four minimum and maximum values (bipolar distribution case) of voltage (Ad-Hoc Voltage) and Laplacian (Ad-Hoc Laplacian). The voltage-to-current and Laplacian techniques were applied also to this montage, which reproduces a bipolar distribution and where the applied current depend on the EEG.
- The ring configurations 4 × 1, 4 × 2, 5 × 1 (5, 6, 6 electrodes) were used for the '*sink-to-concentric ring*' technique when a EEG monopolar scalp distribution was observed for the modeled source direction (Ad-Hoc voltage only in the radial case) and where the applied current does not depend on the EEG. One cathode selected as the EEG electrode with the maximum voltage (Ad-Hoc voltage) and the anode ring with a fixed radius (around 3 cm).

Model-based approaches. Model-based approaches were implemented here only as performance references against the model-free approaches (table 1). The method to rigorously optimize tES based on a known head model and target, and with arbitrary constraints on number of electrodes and electrode currents, was previously described [5] and reproduced here allowing the use of either 8 electrodes, for targeting based optimization, or 2 electrodes, for intensity based optimization. We have previously shown that this form of electrode number restriction will not significantly reduce performance based on the optimization criterion [5, 62].

Scalp potentials generated by tES. In each stimulation case, we predicted the voltage generated on the scalp by the stimulation. By contrasting this with the scalp potentials generated by the dipole sources, we are able to ask if and how homology between tES indicted scalp potential and EEG influences resulting performance.

Quantitative performance analysis. We considered the following parameters to quantify the dose delivered into the brain:

- *Intensity*: the criterion of intensity for each stimulation was identified as the electric field (EF) magnitude generated in the central voxel of the source location. Since the total current was fixed in all cases (1 mA) this allowed comparison of intensity optimization at the target location across montages.
- *Focality*: we considered the ratio between the EF Magnitude at the target location and the mean electric field across the gray matter (mean EF magnitude, voxel wide average cross gray matter), an index of stimulation focality.
- *Directionality*: for all the model solutions we calculated the angle between the $\overrightarrow{EF}$ generated by tES and dipole source vectors

$$\text{Tangential: } \theta(\overrightarrow{EF}, \vec{s}_{\text{tangential}}) = \theta(\overrightarrow{EF}, \overrightarrow{e_y}) = \text{acos}\left(\frac{\Delta y_{\overrightarrow{EF}}}{\pm\sqrt{\Delta x_{\overrightarrow{EF}}^2 + \Delta y_{\overrightarrow{EF}}^2 + \Delta z_{\overrightarrow{EF}}^2}}\right),$$

$$\text{Radial: } \theta(\overrightarrow{EF}, \vec{s}_{\text{radial}}) = \theta(\overrightarrow{EF}, \overrightarrow{e_z}) = \text{acos}\left(\frac{\Delta z_{\overrightarrow{EF}}}{\pm\sqrt{\Delta x_{\overrightarrow{EF}}^2 + \Delta y_{\overrightarrow{EF}}^2 + \Delta z_{\overrightarrow{EF}}^2}}\right).$$

Results

EEG Simulation

To subsequently inform tES, scalp potentials were simulated using either a tangentially-oriented (parallel to the scalp surface) or radially-oriented (normal to the scalp surface) dipole (figure 2, top). The first one produced a dipolar scalp distribution, positive on the frontal section of the scalp and negative on the back of the head, with the zero isopotential line crossing the scalp over the source location. The second one generated a monopolar distribution having the maximum over the dipole on the scalp surface.

EEG guided tES using 330 channels, radially or tangentially-oriented source dipole

We first evaluated EEG-guided tES approaches that utilize the maximum number of available electrodes, under an *a priori* assumption that leveraging more electrodes might enhance performance in EEG-guided tES targeting [83, 84]. In these cases, the tES electrode montage was uniform using 330 electrodes (see methods). Three tES EEG-to-tES mapping techniques (the method which determines the voltage or current set at each electrode based on the EEG signal) were evaluated: voltage-to-voltage (330 electrodes), voltage-to-current (330 electrodes) and 'Laplacian' (290 electrodes as edge electrodes are not available in this case). These model-free approaches were compared to two model-based approaches: optimization of intensity using 2 electrodes, and optimization of focality using 8 electrodes. In every case we evaluated performance for a dipolar source, tangentially (figure 2, left column) or radially (figure 2, right column) oriented and quantified the maximum electric field generated in the brain (max EF magnitude), the electric field magnitude at the dipole target (target EF magnitude), the mean electric field across the gray matter (mean EF magnitude), and the orientation of the electric field at the position of the dipole relative to the dipole (directionality). We also determined the scalp voltage generated by the tES montage in order to quantify homology between the EEG potentials and the voltage in the EEG informed tES.

For the tangentially-directed dipole, all five approaches (three model-free, and two model-based) generated a dipolar distribution on the scalp; for model-free approaches the distribution matched the EEG topography (figure 2), while for model-based approaches it was localized (figure 2). We note that when the distribution of the voltage generated on the scalp by tES matches the EEG topography, the resulting brain current flow is (1) not necessarily targeted with higher accuracy than montages which generate different scalp voltage distribution (2) not necessarily consistent across tES approaches (focality: voltage-to-voltage 0.89, voltage-to-current 1.24, Laplacian 1.92, model-based 2.54 and 2,89; see figure 2 for the scalp voltage distributions and figure 6 for the parameter comparison). For example, the Voltage-to-Voltage approach generated scalp voltages comparable to the EEG, but produces a current flow in the brain that does not affect the target with focality comparable to the other techniques (figure 2, left, row 2). The voltage-to-voltage approach is not further considered. The voltage-to-current and Laplacian techniques both produced current intensity at the target that is close to the maximum brain current intensities and an orientation at the target close to the dipole (figure 2, left). We predicted moderately better focality for the Laplacian approach. Both approaches diffused current in the right hemisphere, anteriorly and posteriorly to the central sulcus, in spite of the target location being in the left somatosensory cortex (figure 2). Given these encouraging results, the need for a high number of electrodes are later considered for the voltage-to-current and Laplacian techniques. The model-based approaches (figure 2, left, bottom two rows) demonstrate higher focality or intensity values, according to the intensity (focality 2.54, intensity 1.22 V m^{-1}) or focality (focality 2.89 and intensity 1.07 V m^{-1}) optimizations. So intensity optimization enhances electric field at the target (14%), while focality optimization minimized mean electric field outside the target (relative to the target electric field, 13%).

For the radially-oriented dipole, the model-free approach using 330 electrodes performed less well than the tangential case. Voltage-to-voltage did not generate an electric field centered at the target location but in the left temporal region (intensity 0.17, focality 1.54; figure 2, right column, second row). Voltage-to-current showed slightly better relative performance concerning Intensity and slightly worse regarding focality (intensity 0.17, focality 1.11; figure 2, right column, third row). Both these tES approaches generate a unipolar scalp voltage distribution comparable to the EEG. The Laplacian approach generated a bipolar voltage distribution with a negative pole centered on the frontal area of the scalp, absent in the EEG, and

a current flow anterior to the target. These approaches were not considered further. The model-based approaches (figure 2, right, bottom two rows) demonstrate higher focality or intensity values, either for the case of intensity (focality 1.43 and intensity 0.93 V m^{-1}) or focality (focality 3.94 and intensity 0.75 V m^{-1}) optimizations. So the intensity optimization enhances electric field at the target but polarizes much of the hemisphere (figure 2, second-last row). Focality optimization is only moderately targeted (figure 2, last row).

In summary, carrying out computational modeling of EEG guided tES, we found no evidence the tES approaches that produce scalp voltages that replicate the EEG or provide enhanced brain targeting. The performance of various EEG-to-tES mapping approaches may depend on the general features of the scalp EEG (dipole or unipolar distribution) such that we continue to separately consider the radial and tangential source cases—including when we propose Ad-Hoc approaches. When ~300 electrodes are used, Laplacian mapping, followed by voltage-to-current generate better performance than voltage-to-voltage. We next consider the role of electrode number.

EEG guided tES using sub-set of uniform-distributed channels, tangentially-oriented source dipole

For the case of a tangentially-orientated dipole, we further considered the voltage-to-current and Laplacian techniques, reducing the number of tES electrodes from 256, to 128, to 64, to 32, to 16, and to 8 (figure 3). We emphasize that these electrode montages were always uniform, and electrode selections were not informed by the EEG (in contrast to Ad-Hoc approaches). We observed that focality decreases dramatically as electrode number is reduced below 32 for the voltage-to-current method and below 64 for the Laplacian method (figures 3, 4 and 6).

We therefore conclude that for the most promising uniform electrode montage approach, a relatively high number of electrodes are needed. Yet, model-based approaches suggest that optimized performance can be obtained with a low number of electrodes (figure 2, bottom two rows; [5, 62]). These results encouraged us to consider non-uniform based electrode montage based on Ad-Hoc selection next.

EEG guided tES using an Ad-Hoc selection of channels, tangentially and radially-oriented source dipole

With our Ad-Hoc technique, the selection of electrodes (see sink-to-sink and sink-to-ring paragraphs in the EEG-to-tES mapping techniques section) is based on the EEG.

For the case of a tangentially-oriented dipole (bipolar EEG) we considered an electrode montage selection process based on selecting the electrode with the highest EEG voltage (figure 5, first column) or highest EEG Laplacian (figure 5, second column). When electrodes were selected based on voltage, voltage-to-current was used to determine tES electrode current. When electrodes were selected based on EEG Laplacian, Laplacian technique was used to determine tES electrode current. In each case we considered a selection of 8, 4, or 2 electrodes for tES, with 1 mA distributed across all electrodes. In the case of 2 electrodes (bottom row), the current applied to the electrodes was fixed at 1 mA, so the technique is sink-to-sink. Interestingly, all Ad-Hoc approaches that were tested (figure 5) showed a better combination between intensity and focality (figure 6, top) than the one obtained with the uniform electrode montages (figure 2). Thus using less electrodes (2–8) but selecting electrodes based on the EEG (figure 5), enhances performance. Moreover, for both Ad-Hoc approaches, reducing the number of electrodes from 8 to 2 where cathode and anode are placed in the location of the absolute maximum and minimum (sink-to-sink technique), enhanced performance in regards to intensity, focality and orientation (figures 5 and 6). For sink-to-sink (using just two electrodes) Laplacian EEG based electrode selection (intensity 1.14 V m^{-1}, focality 5.18) produced slightly lower peak at the target with improved focality compared to EEG voltage based electrode selection (intensity 1.21 V m^{-1}, focality 2.75).

For the case of radially-oriented dipole (unipolar EEG) we considered an electrode montage selection process based on selecting an electrode with the highest EEG voltage (figure 5, third columns) or electrodes with the highest EEG Laplacian (figure 5, fourth column). When electrodes were selected based on EEG voltage, a ring montage was used with 1 mA applied to the center electrodes. When electrodes were selected based on EEG Laplacian, Laplacian technique was used to determine tES electrode current—an identical method as for the tangential case. Again, we discovered that using less electrodes but selecting electrodes based on the EEG (4 × 1: focality 4.4, intensity 0.31 V m^{-1}, directionality 9.3°; figure 5) resulted in a dramatic increase of focality compares to approaches using even hundreds of electrodes (voltage-to-current technique with 256 electrodes: focality 1.6, intensity 0.54 V m^{-1}; figure 2). The concentric ring montage produced the best targeting; performance was already optimal with 4 × 1 (focality 4.4) such that adding more electrodes, either cathodes or anodes, did not significantly change brain current flow (5 × 1: focality 4.0, intensity 0.32 V m^{-1}, directionality 9°; 4 × 2: focality 4.40, intensity: 0.31 V m^{-1}, directionality 9°; figure 5). In comparison, the Laplacian method was less focal when applying 8 electrodes (focality 2.30, intensity 0.62 V m^{-1}, directionality 34°), and performance even degraded as the number of electrodes decreased (4 electrodes: focality 2.30, intensity 0.31 V m^{-1}, directionality 26°; 2 electrodes: focality 1.5, intensity 0.12 V m^{-1}, directionality 22°; figure 5).

In summary, we report that the Ad-Hoc approach improves performance over uniform electrode montage, and in contrast to uniform electrode montage, requires fewer electrodes (2–8 depending on approach). In the case of bipolar EEG, Laplacian electrode selection with two electrodes (Sink-to-Sink) is superior based on brain targeting/intensity and low-electrode count among Ad-Hoc approaches tested. Similarly, in the case of unipolar EEG, concentric ring with 4 × 1 montage is superior. The Laplacian Ad-Hoc method (Laplacian electrode and current selection) with 8 electrodes is the most robust approach across methods in which the current was based on the EEG.

Overall performance comparison with model-free uniform electrode, model-free Ad-Hoc, and model-based techniques

Overall performance was compared across all tested montages quantifying intensity at target versus focality, as this represent

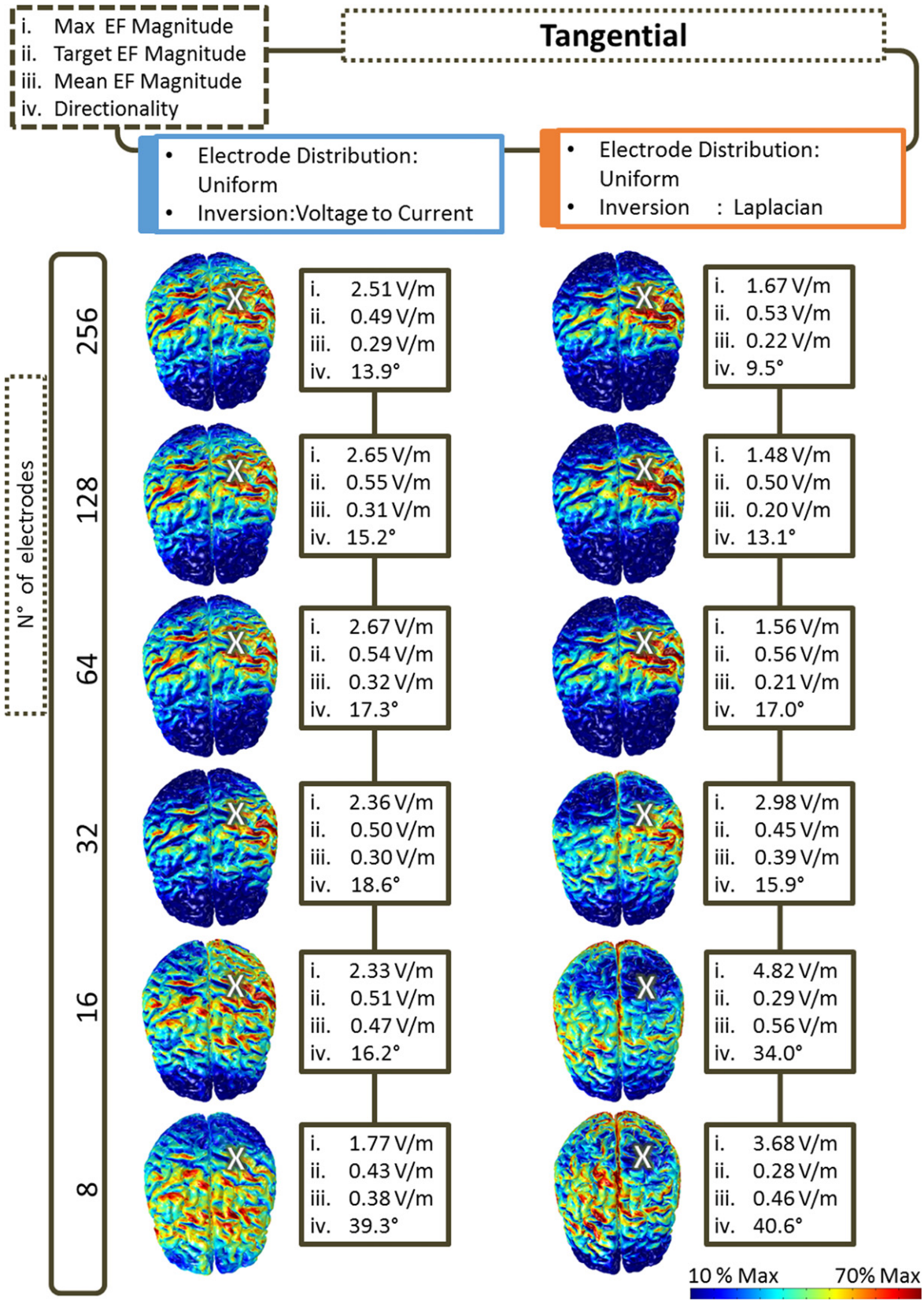

Figure 3. Voltage-to-current and Laplacian EEG-to-tES mapping techniques. Tangential comparison using uniform electrode montages.

a fundamental trade-off in tES [5]. For a tangentially-directed dipole, two model-free Ad-Hoc approaches with just 2 electrodes produced maximum target intensity compared to model-based optimization: the montages with sink-to-sink current application, having electrodes selected in function of the EEG voltages (intensity 1.21 V m^{-1}, focality 2.75; figure 5) and the Laplacian (intensity 1.14 V m^{-1}, focality 5.18; figure 5). The latter with slightly less target intensity but

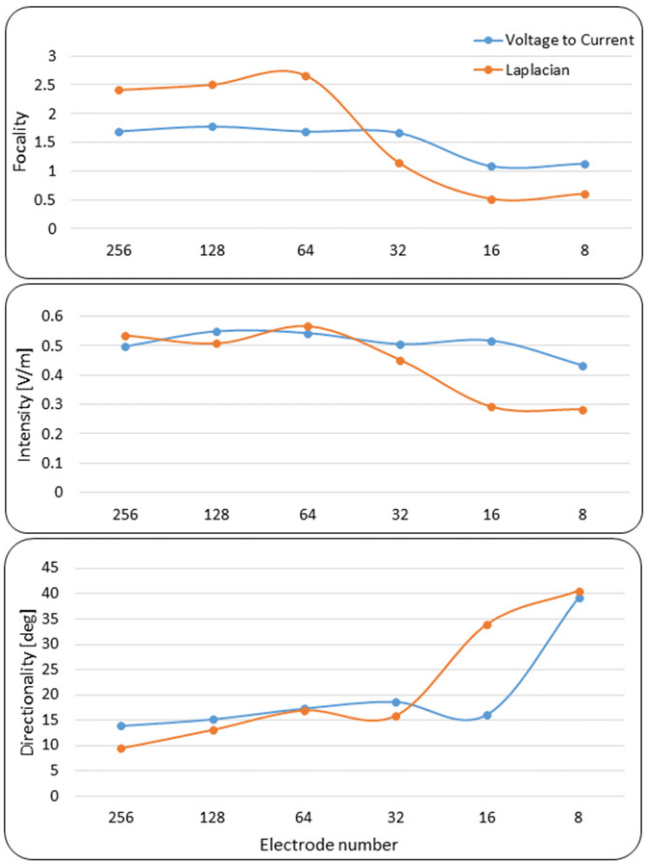

Figure 4. Voltage-to-current and Laplacian EEG-to-tES mapping techniques. Tangential comparison evaluating focality, intensity and directionality in function of the used sub-set of uniform-distributed channels.

almost double focality. The improved focality compared to model-based focality optimization should be understood as reflecting a difference in how focality is scored; model-based approaches guarantee best performance given a specific cost function [5]. Approaches with uniform electrode montage generally underperformed; among them Laplacian current application with 64 or greater electrodes produced reasonable focality (focality $\sim$ 2.5) and around half intensity (0.52, 0.50 and 0.53 V m^{-1}) of the sink-to-sink Ad-Hoc approaches (1.14 and 1.21 V m^{-1}).

For a radially-directed dipole, the model-free Ad-Hoc ring based approached resulted in focality around ten times higher (focality $\sim$40) than other approaches (max focality 4 for the model-based approach). Here again improvement against model-based focality optimization should be read as based on the cost function which provided the numerical optimization [5, 6]. Model-based tES also produced higher intensities at the target. The Ad-Hoc Laplacian based method with 8 electrodes was the closest performance (intensity 0.62 V m^{-1}, focality 2.3) to model-based optimization (intensity 0.75 V m^{-1}, focality 3.9).

Discussion

Our approach for model-free targeting of tES by EEG was previously presented in abstract form [85].

The theoretical benefit to leveraging EEG to guide tES is entirely dependent on the strategy (methodological approach) used and constraints on the stimulation technology (pad versus HD style electrode, 2 electrodes versus arrays; [86]) as well at the nature of the EEG. Through a computational analysis, this paper develops a first step toward strategies for EEG guided tES expressly to exclude models, based on examples from single dipoles. We demonstrate remarkable overall brain targeting performance with model-free approaches that require few (2–8) electrodes. Our novel Ad-Hoc approaches are optimized based on distinguishing two typologies of scalp EEG distributions: monopolar as in the radially-oriented dipole and bipolar as in the tangentially-oriented dipole; the former indicating a tES concentric ring approach targeted around EEG voltage minimum and the latter a tES sink-to-sink targeted around the EEG Laplacian (figure 5). Alternatively, without distinguishing these general EEG distributions, tES based on EEG Laplacian with 8 electrodes provides high performance (figure 5, right). Our results cast doubt on the notion that an optimal tES strategy should provide a scalp voltage distribution that approximates the EEG (e.g., voltage-to-voltage shows high homology between EEG and tES scalp voltage but poor targeting, figure 2). And our results show that many (hundreds) of tES electrodes are not necessarily needed if the right strategy is used (compare performance reliance on high electrode number with uniform approaches in figure 3 with low electrode number for Ad-Hoc approaches in figure 5). Additional features of our approach are discussed.

The goal of using EEG to design and optimize tES is not new and it is based on the reciprocity application [1]. But the adoption remains investigational [7, 8, 14, 38] and limited (see introduction, [9–13, 87]).

We discuss model-free approaches in regards to features that support adoption:

(1) No need for subject-specific imaging.
(2) Applicable with any EEG montage.
(3) Limiting the number of stimulation electrodes to the extent desired.
(4) Account for brain neural source orientation as well as position.
(5) Balance tES optimization for focality versus intensity.
(6) Apply to any static (tDCS) or time-dependent application (tACS, tRNS, tPCS).
(7) Lend itself to various forms of EEG analysis.
(8) Allow current limits based on tolerability standards.
(9) Remain computationally light.

Methods that require subject-specific anatomical imaging are burdensome [2, 88, 89]. The acquisition of sufficiently precise imaging data is costly and often impractical. Subject specific imaging implies methods to model the head, which requires algorithms for tissue segmentation [90], as well as forward and/or inverse current flow simulations. Because of uncertainty, these models rely on assumptions about tissue segmentation and conductivity, the nature of brain electrical sources, etc. Even if a standard template head is used (ICBM152; New York Head; [25, 91]) the inverse problem

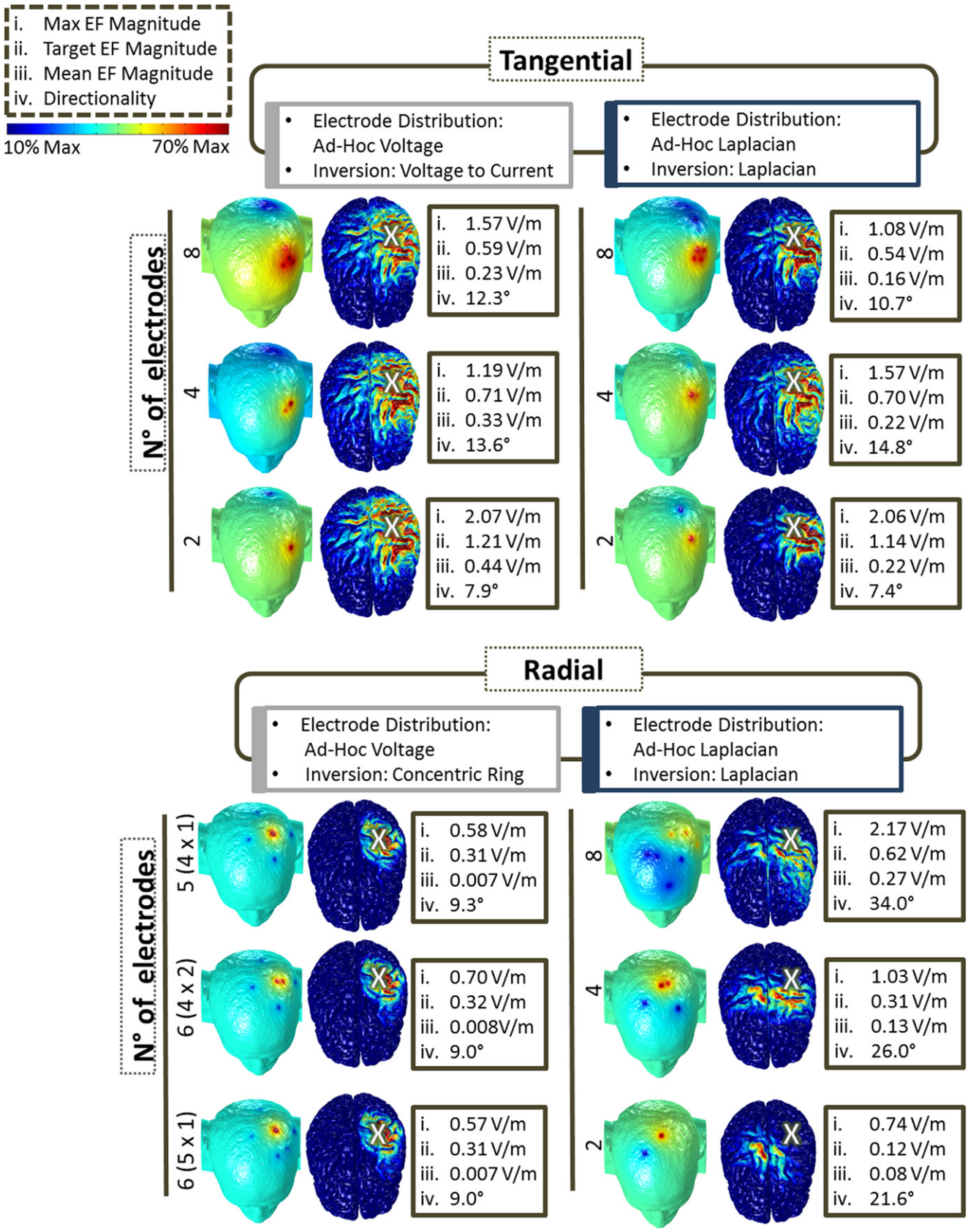

Figure 5. Minimal functional sets of HD electrodes. For both the dipole directions, tangential and radial, groups of two, four and eight HD electrodes were placed over the peaks of the scalp voltage distribution generated by the source (voltage peaks) and over the peaks of the Laplacian distribution (Laplacian peaks).

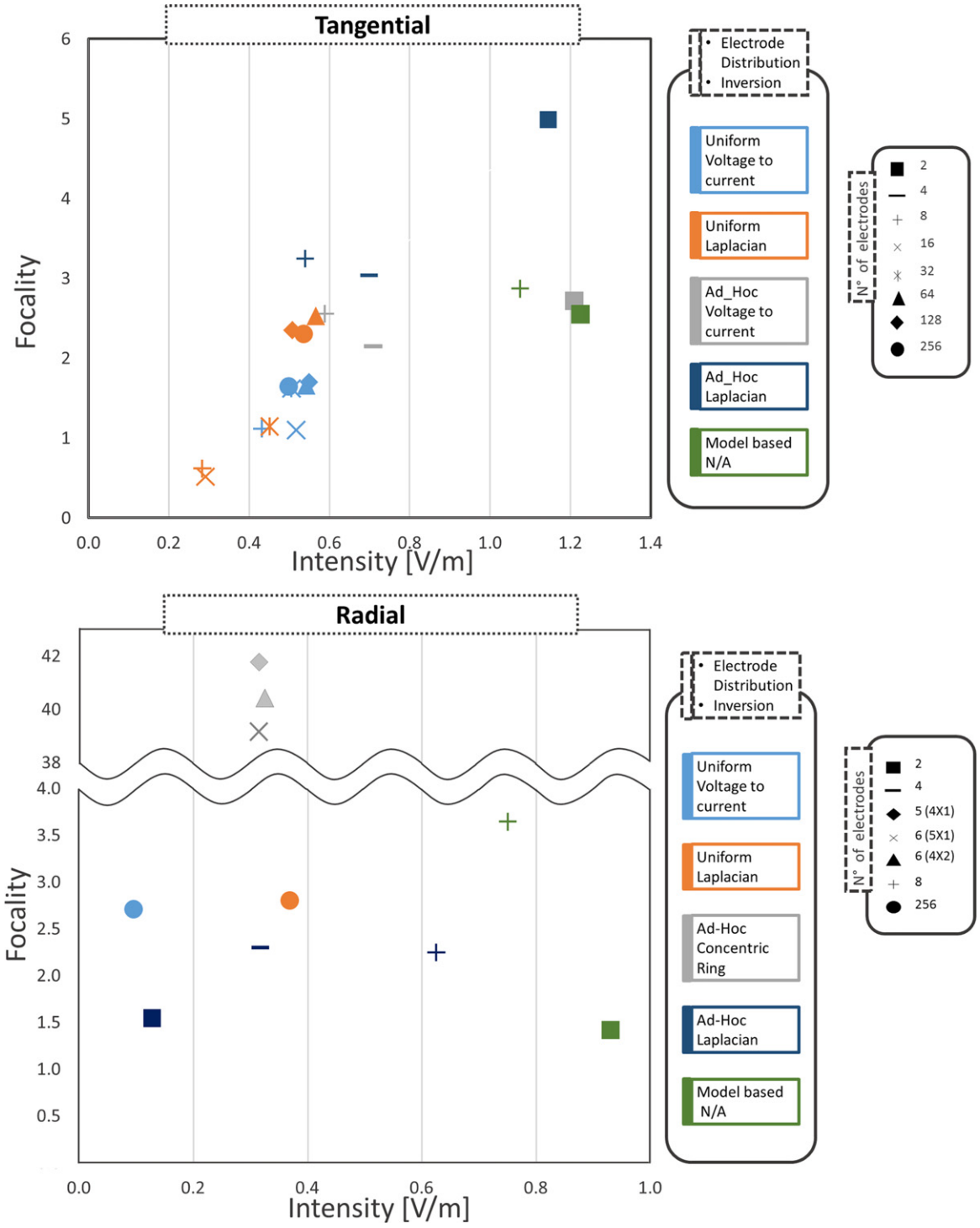

Figure 6. Tangential and radial EEG-to-tES mapping cases chart. Scatter plot showing a quantitative tangential and radial montage comparison. Value of the electric field in the source location on the *X* axis and an index of focality on the *Y* axis, calculated as the ratio between the value of the electric field in the source location and the total electric field delivered into the gray matter. In the legend of the chart, colors mean the positioning of the electrodes and the EEG-to-tES mapping method applied to set the current intensity at each electrode. The shape of the symbols indicate the number of electrodes used in each stimulation.

which relates EEG potentials to anatomical tES targets is ill-posed and thus may yield inaccurate solutions [92–95]. A method to guide tES by EEG without the need for a head model would accelerate adoption and would hopefully lead toward more clinically efficacious treatments. Yet research suggests both interpretation of EEG and design of tES [25, 91] benefit from subject specific head models. Model-free EEG guided tES is a physiological, data-driven technique that attempts to circumvent these problems by exploiting the fact that information about head anatomy and source

orientation is intrinsically present in the EEG measurement. Leveraging this information may obviate the need for an MRI-based head model.

Various EEG electrode deployments are used, ranging from the common 10/10 and 10/20, to concentric rings, to custom configurations [93, 96–98]. These configurations are based on set-up expediency and in practice placements are approximated (e.g., using pre-loaded caps). A method that is specific to one configuration or requires registering each electrode location with a model of the head is impractical. Our approaches for model-free EEG guided tES inherently configures to any EEG deployment, even if arbitrary.

Decreasing the number of tES channels increases practicality [99]. In addition to reduced hardware complexity, whereas a few non-ideal EEG electrodes do not necessarily compromise an entire recording, for tES even one poor electrode contact can compromise tolerability [40, 77, 100]. In contrast to EEG, where broad coverage and high density enhances imaging [36, 83], for tES low-electrode deployments can approach optimality if the target is known (model-based approaches in figure 2; [5, 62, 101]). Whereas approaches based on uniform tES electrode configuration quickly degrade in performance with reduced number of electrodes (figure 3), we show that Ad-Hoc approaches achieve reasonable results targeting with just two and five electrodes for tangential and radial modeled source directions, respectively (figure 5).

Previous studies showed how tES montages using two HD electrodes and a concentric-ring HD (e.g., 4 × 1) montage can produce targeted tangential and radial brain current flow, respectively [62, 63]. Here we suggest Ad-Hoc approaches to select and configure these tES montages guided by the EEG, and show performance approaching with the model- based optimization (figure 5). The applied tES current is not only guided to the target location, but also matches the dipole orientation (directionality; figure 5; [48]). The 4 × 1 and the sink-to-sink Ad-Hoc Laplacian montages generated current flows having respectively a solid angle (directionality) of 9.3° with the radial and 7.4° with the tangential directions.

While simple to implement, the result of the Ad-Hoc model-free EEG guided tES is not trivial. tES optimization needs to balance the antagonistic constraints of intensity and focality; with head model-based approaches this requires committing to the targeted brain region *a priori* [5].

The presented techniques may also find application to alternating current stimulation paradigms where one aims to modulate the amplitude of an observed brain rhythm [102–105]. For example, stimulation at the low frequencies characteristic of the EEG has been shown to selectively modulate oscillatory brain activity (e.g., alpha frequency stimulation to influence alpha related activity [106, 107]). tACS has been applied at both fixed or individualized frequencies [32]. However, optimization of the placement of tACS electrodes remains largely unexplored. The approach presented here may potentially optimize the modulation of oscillatory brain activity by stimulating at sites exhibiting maximal oscillatory amplitude at the frequency-of-interest.

The EEG is inherently time variant. Our model-free techniques are based on an instantaneous representation of the scalp voltage at each electrode and may thus be applied in a time-varying manner that 'tracks' the dynamic EEG pattern. Moreover, the technique is compatible with numerous commonplace EEG preprocessing methods such as basis decomposition or component analysis [108–110]. For example, our approach could be applied to a particular (spatial) EEG component which is implicated in the disorder or behavior-of-interest.

The proposed model-free approaches for EEG guided tES can be implemented with any Ad-Hoc current limits applied per electrode and/or in sum (see normalization in methods). These current limits are typically based on empirical experience (what is tolerated), and historical norms [49–51].

In addition, reducing the number of tES electrodes may reduce the burden in regards to hardware and set-up, but increases current per electrode. Our Ad-Hoc approaches allow for some flexibility in this regard.

Our Ad-Hoc approaches depend on identifying a characteristic dipole signature (radially or tangentially directed) in the EEG, and we verify performance only for a single dipole case. However, the characterization of EEG assuming a dipole EEG topography is ubiquitous (though with methodological considerations; [111–114]) leveraging conventional signal processing such as averaging (repeated evoked response), filtering, ICA, etc [110, 115–117]; mapping EEG to tES parameters based on dipoles, when they are identified in the EEG, is a rational first approximation [111–114]. The robustness of the technique across brain regions remains to be verified, but bipolar and concentric ring stimulation montages are robust across underlying anatomy [45, 118]. In this sense, use of low-electrode numbers (e.g., two or five) may be a further generalization advantage over stimulation approaches relying on a high number of electrodes.

Our approach cannot overcome limitations inherent in brain neurophysiology and/or EEG that result if a diffuse source of activity and ambiguous detection. These issues have for decades motivated imaging research [119–131]. Our emphasis here is an immediately tractable and customizable approach that at improves on current efforts that use large pads and no spatial optimization. Identification of (two) EEG channels with maximum activity is common [132–134], thus the presence of multiple (dipole) sources does not diminish our protocol to target one identified source. Evidently the scalp EEG measurements vary in time, but standard time-domain signal processing can be used to select channels [108, 135–139]. Ultimately, adoption of our approach to refine clinical treatments with tES/tDCS, depends on still further assumptions such as if targeted and individualized cortical stimulation of preferred over brain-wide stimulation. For the noted limits of our approach, it is rationale, adoptable, and testable.

The proposed approach is essentially a data-driven lookup table for designing tES montages, and thus requires minimal computational resources. It is also amenable to real-time adaptive operation limited only by how fast the electrode selection can be performed; though it is critical in such cases where interactions between stimulation and recording systems (e.g., skin erythema by tES changing EEG pick-up) need to be explicitly addressed. In summary, we proposed a simple and broadly deployable method for EEG guided tES.

Acknowledgments

The authors would like to thank Dr Camillo Porcaro and Ole Seibt for their valuable scientific contribution. MB is supported by the NIH, NSF, and DoD (AFOSR).

COI

MB has equity in Soterix Medical Inc. The City University of New York has patents on brain stimulation with MB as inventor.

References

[1] Rush S and Driscoll D A 1969 EEG electrode sensitivity–an application of reciprocity *IEEE Trans. Bio-Medical Eng.* **16** 15–22

[2] Dmochowski J P *et al* 2013 Targeted transcranial direct current stimulation for rehabilitation after stroke *NeuroImage* **75** 12–9

[3] Galletta E E *et al* 2015 Use of computational modeling to inform tDCS electrode montages for the promotion of language recovery in post-stroke Aphasia *Brain Stimulation* **8** 1108–15

[4] Burnap R L and Sherman L A 1991 Deletion mutagenesis in *Synechocystis sp*. PCC6803 indicates that the Mn-stabilizing protein of photosystem II is not essential for O_2 evolution *Biochemistry* **30** 440–6

[5] Dmochowski J P, Datta A, Bikson M, Su Y and Parra L C 2011 Optimized multi-electrode stimulation increases focality and intensity at target *J. Neural Eng.* **8** 046011

[6] Sadleir R J, Vannorsdall T D, Schretlen D J and Gordon B 2012 Target optimization in transcranial direct current stimulation *Frontiers Psychiatry* **3** 90

[7] Heller L and van Hulsteyn D B 1992 Brain stimulation using electromagnetic sources: theoretical aspects *Biophys. J.* **63** 129–38

[8] Ziegler E *et al* 2014 A finite-element reciprocity solution for EEG forward modeling with realistic individual head models *NeuroImage* **103** 542–51

[9] Assenza G *et al* 2014 Efficacy of cathodal transcranial direct current stimulation in drug-resistant epilepsy: a proof of principle *Conf. Proc.: Annual Int. Conf. IEEE Engineering in Medicine and Biology Society* vol 2014 pp 530–3

[10] Cunillera T, Brignani D, Cucurell D, Fuentemilla L and Miniussi C 2015 The right inferior frontal cortex in response inhibition: a tDCS-ERP co-registration study *NeuroImage* **15** S1053–8119

[11] Tekturk P *et al* 2016 Transcranial direct current stimulation improves seizure control in patients with Rasmussen encephalitis *Epileptic Disord.* **18** 58–66

[12] Krause V, Meier A, Dinkelbach L and Pollok B 2016 Beta band transcranial alternating (tACS) and direct current stimulation (tDCS) applied after initial learning facilitate retrieval of a motor sequence *Frontiers Behav. Neurosci.* **10** 4

[13] Neuling T, Rach S, Wagner S, Wolters C H and Herrmann C S 2012 Good vibrations: oscillatory phase shapes perception *NeuroImage* **63** 771–8

[14] Ha U, Lee Y, Kim H, Roh T, Bae J, Kim C and Yoo H J 2015 A wearable EEG-HEG-HRV multimodal system with simultaneous monitoring of tES for mental health management *IEEE Trans. Biomedical Circuits Syst.* **9** 758–66

[15] Roh T, Song K, Cho H, Shin D and Yoo H J 2014 A wearable neuro-feedback system with EEG-based mental status monitoring and transcranial electrical stimulation *IEEE Trans. Biomedical Circuits Syst.* **8** 755–64

[16] Laarne P, Hyttinen J, Dodel S, Malmivuo J and Eskola H 2000 Accuracy of two dipolar inverse algorithms applying reciprocity for forward calculation *Comput. Biomedical Res. Int. J.* **33** 172–85

[17] Strobbe G *et al* 2014 Bayesian model selection of template forward models for EEG source reconstruction *NeuroImage* **93** 11–22

[18] Marangolo P *et al* 2016 Bilateral transcranial direct current stimulation language treatment enhances functional connectivity in the left hemisphere: preliminary data from Aphasia *J. Cogn. Neurosci.* **28** 724–38

[19] Tecchio F *et al* 2015 Brain plasticity effects of neuromodulation against multiple sclerosis fatigue *Frontiers Neurology* **6** 141

[20] Brunoni A R *et al* 2012 Clinical research with transcranial direct current stimulation (tDCS): challenges and future directions *Brain Stimulation* **5** 175–95

[21] Sasaki R, Miyaguchi S, Kotan S, Kojima S, Kirimoto H and Onishi H 2016 Modulation of cortical inhibitory circuits after cathodal transcranial direct current stimulation over the primary motor cortex *Frontiers Hum. Neurosci.* **10** 30

[22] Tecchio F *et al* 2014 Multiple sclerosis fatigue relief by bilateral somatosensory cortex neuromodulation *J. Neurology* **261** 1552–8

[23] Costanzo F *et al* 2016 Reading changes in children and adolescents with dyslexia after transcranial direct current stimulation *Neuroreport* **27** 295–300

[24] Frohlich F *et al* 2016 Exploratory study of once-daily transcranial direct current stimulation (tDCS) as a treatment for auditory hallucinations in schizophrenia *Eur. Psychiatry: J. Assoc. Eur. Psychiatrists* **33** 54–60

[25] Datta A, Truong D, Minhas P, Parra L C and Bikson M 2012 Inter-individual variation during transcranial direct current stimulation and normalization of dose using MRI-derived computational models *Frontiers Psychiatry* **3** 91

[26] Lopez-Alonso V, Fernandez-Del-Olmo M, Costantini A, Gonzalez-Henriquez J J and Cheeran B 2015 Intra-individual variability in the response to anodal transcranial direct current stimulation *Clin. Neurophysiology: Official J. Int. Fed. Clin. Neurophysiology* **126** 2342–7

[27] Wiethoff S, Hamada M and Rothwell J C 2014 Variability in response to transcranial direct current stimulation of the motor cortex *Brain Stimulation* **7** 468–75

[28] Coenen V A *et al* 2016 One-pass deep brain stimulation of dentato-rubro-thalamic tract and subthalamic nucleus for tremor-dominant or equivalent type Parkinson's disease *Acta Neurochirurgica* **158** 773–81

[29] Krall S C, Volz L J, Oberwelland E, Grefkes C, Fink G R and Konrad K 2016 The right temporoparietal junction in attention and social interaction: a transcranial magnetic stimulation study *Hum. Brain Mapp.* **37** 796–807

[30] Yarossi M, Adamovich S and Tunik E 2014 Sensorimotor cortex reorganization in subacute and chronic stroke: a neuronavigated TMS study *Conf. Proc.: Annual Int. Conf. IEEE Engineering in Medicine and Biology Society* vol 2014 pp 5788–91

[31] Kious B M, Jimenez-Shahed J and Shprecher D R 2016 Treatment-refractory Tourette syndrome *Progress Neuro-Psychopharmacology Biol. Psychiatry* **16** S0278–5846

[32] Zaehle T, Rach S and Herrmann C S 2010 Transcranial alternating current stimulation enhances individual alpha activity in human EEG *PloS One* **5** e13766

[33] Castillo Saavedra L *et al* 2014 QEEG indexed frontal connectivity effects of transcranial pulsed current stimulation (tPCS): a sham-controlled mechanistic trial *Neurosci. Lett.* **577** 61–5

[34] Hoy K E, Bailey N W, Arnold S L and Fitzgerald P B 2015 The effect of transcranial Direct Current Stimulation on gamma activity and working memory in schizophrenia *Psychiatry Res.* **228** 191–6

[35] Li G M 1989 Studies on the medicinal species of Bupleurum in Shanxi, Gansu, Ningxia, Qinghai and Xingjiang *Zhongguo Zhong Yao Za Zhi.* **14** 262–7 [in Chinese]
[36] Song M, Shin Y and Yun K 2014 Beta-frequency EEG activity increased during transcranial direct current stimulation *Neuroreport* **25** 1433–6
[37] Van Doren J, Langguth B and Schecklmann M 2014 Electroencephalographic effects of transcranial random noise stimulation in the auditory cortex *Brain Stimulation* **7** 807–12
[38] Roy A, Baxter B and He B 2014 High-definition transcranial direct current stimulation induces both acute and persistent changes in broadband cortical synchronization: a simultaneous tDCS-EEG study *IEEE Trans. Bio-Medical Eng.* **61** 1967–78
[39] Borckardt J J *et al* 2012 A pilot study of the tolerability and effects of high-definition transcranial direct current stimulation (HD-tDCS) on pain perception *J. Pain: Official J. Am. Pain Soc.* **13** 112–20
[40] Minhas P *et al* 2010 Electrodes for high-definition transcutaneous DC stimulation for applications in drug delivery and electrotherapy, including tDCS *J. Neurosci. Methods* **190** 188–97
[41] Caparelli-Daquer E M *et al* 2012 A pilot study on effects of 4 × 1 high-definition tDCS on motor cortex excitability *Conf. Proc.: Annual Int. Conf. IEEE Engineering in Medicine and Biology Society* vol 2012 pp 735–8
[42] Helfrich R F *et al* 2014 Selective modulation of interhemispheric functional connectivity by HD-tACS shapes perception *PLoS Biol.* **12** e1002031
[43] Kuo H I *et al* 2013 Comparing cortical plasticity induced by conventional and high-definition 4 × 1 ring tDCS: a neurophysiological study *Brain Stimulation* **6** 644–8
[44] Nikolin S, Loo C K, Bai S, Dokos S and Martin D M 2015 Focalised stimulation using high definition transcranial direct current stimulation (HD-tDCS) to investigate declarative verbal learning and memory functioning *NeuroImage* **117** 11–9
[45] Shekhawat G S, Sundram F, Bikson M, Truong D, De Ridder D, Stinear C M, Welch D and Searchfield G D 2015 Intensity, duration, and location of high-definition transcranial direct current stimulation for tinnitus relief *Neurorehabil Neural Repair.* **30** 349–59
[46] Kempe R, Huang Y and Parra L C 2014 Simulating pad-electrodes with high-definition arrays in transcranial electric stimulation *J. Neural Eng.* **11** 026003
[47] Cancelli A, Cottone C, Di Giorgio M, Carducci F and Tecchio F 2015 Personalizing the electrode to neuromodulate an extended cortical region *Brain Stimulation* **8** 555–60
[48] Rahman A *et al* 2013 Cellular effects of acute direct current stimulation: somatic and synaptic terminal effects *J. Physiol.* **591** 2563–78
[49] Bikson M, Datta A and Elwassif M 2009 Establishing safety limits for transcranial direct current stimulation *Clin. Neurophysiology: Official J. Int. Fed. Clin.Neurophysiology* **120** 1033–4
[50] Nitsche M A, Liebetanz D, Lang N, Antal A, Tergau F and Paulus W 2003 Safety criteria for transcranial direct current stimulation (tDCS) in humans *Clin. Neurophysiology: Official J. Int. Fed. Clin. Neurophysiology* **114** 2220–2
[51] Liebetanz D, Koch R, Mayenfels S, Konig F, Paulus W and Nitsche M A 2009 Safety limits of cathodal transcranial direct current stimulation in rats *Clin. Neurophysiology: Official J. Int. Fed. Clin. Neurophysiology* **120** 1161–7
[52] Schmitt H, Ferdinand N K and Kray J 2014 Age-differential effects on updating cue information: evidence from event-related potentials *Cogn. Affective Behav. Neurosci.* **14** 1115–31
[53] Gonzalez-Roldan A M, Cifre I, Sitges C and Montoya P 2016 Altered dynamic of EEG oscillations in fibromyalgia patients at rest *Pain Med.* pnw023 (doi:10.1093/pm/pnw023)
[54] Vecchio F *et al* 2016 Cortical connectivity and memory performance in cognitive decline: a study via graph theory from EEG data *Neuroscience* **316** 143–50
[55] Tomasevic L *et al* 2013 Cortico-muscular coherence as an index of fatigue in multiple sclerosis *Multiple Sclerosis* **19** 334–43
[56] Smits F M, Porcaro C, Cottone C, Cancelli A, Rossini P M and Tecchio F 2016 Electroencephalographic fractal dimension in healthy ageing and Alzheimer's disease *PloS One* **11** e0149587
[57] Cogliati Dezza I *et al* 2015 Functional and structural balances of homologous sensorimotor regions in multiple sclerosis fatigue *J. Neurology* **262** 614–22
[58] Dmochowski J P, Bikson M, Datta A, Richardson J, Fridriksson J and Parra L C 2012 On the role of electric field orientation in optimal design of transcranial current stimulation *Conf. Proc.: Annual Int. Conf. of the IEEE Engineering in Medicine and Biology Society* vol 2012 pp 6426–9
[59] Reato D, Gasca F, Datta A, Bikson M, Marshall L and Parra L C 2013 Transcranial electrical stimulation accelerates human sleep homeostasis *PLoS Comput. Biol.* **9** e1002898
[60] Bikson M *et al* 2008 Transcranial direct current stimulation for major depression: a general system for quantifying transcranial electrotherapy dosage *Curr. Treat. Options Neurology* **10** 377–85
[61] Datta A, Baker J M, Bikson M and Fridriksson J 2011 Individualized model predicts brain current flow during transcranial direct-current stimulation treatment in responsive stroke patient *Brain Stimulation* **4** 169–74
[62] Datta A, Bansal V, Diaz J, Patel J, Reato D and Bikson M 2009 Gyri-precise head model of transcranial direct current stimulation: improved spatial focality using a ring electrode versus conventional rectangular pad *Brain Stimulation* **2** 201–7
[63] Datta A, Elwassif M, Battaglia F and Bikson M 2008 Transcranial current stimulation focality using disc and ring electrode configurations: FEM analysis *J. Neural Eng.* **5** 163–74
[64] Faria P, Hallett M and Miranda P C 2011 A finite element analysis of the effect of electrode area and inter-electrode distance on the spatial distribution of the current density in tDCS *J. Neural Eng.* **8** 066017
[65] Kabakov A Y, Muller P A, Pascual-Leone A, Jensen F E and Rotenberg A 2012 Contribution of axonal orientation to pathway-dependent modulation of excitatory transmission by direct current stimulation in isolated rat hippocampus *J. Neurophysiology* **107** 1881–9
[66] Parazzini M, Fiocchi S, Rossi E, Paglialonga A and Ravazzani P 2011 Transcranial direct current stimulation: estimation of the electric field and of the current density in an anatomical human head model *IEEE Trans. Bio-Medical Eng.* **58** 1773–80
[67] Wagner S *et al* 2014 Investigation of tDCS volume conduction effects in a highly realistic head model *J. Neural Eng.* **11** 016002
[68] Wagner T, Fregni F, Fecteau S, Grodzinsky A, Zahn M and Pascual-Leone A 2007 Transcranial direct current stimulation: a computer-based human model study *NeuroImage* **35** 1113–24
[69] Berg P and Scherg M 1994 A multiple source approach to the correction of eye artifacts *Electroencephalogr. Clin. Neurophysiol.* **90** 229–41
[70] Probst T, Plendl H, Paulus W, Wist E R and Scherg M 1993 Identification of the visual motion area (area V5) in the human brain by dipole source analysis *Exp. Brain Res.* **93** 345–51
[71] Scherg M and Ebersole J S 1994 Brain source imaging of focal and multifocal epileptiform EEG activity

Neurophysiologie Clinique = Clin. Neurophysiology **24** 51–60
[72] Scherg M and Von Cramon D 1986 Evoked dipole source potentials of the human auditory cortex *Electroencephalogr. Clin. Neurophysiol.* **65** 344–60
[73] Kakigi R and Shibasaki H 1992 Effects of age, gender, and stimulus side on the scalp topography of somatosensory evoked potentials following posterior tibial nerve stimulation *J. Clin. Neurophysiology: Official Publ. Am. Electroencephalographic Soc.* **9** 431–40
[74] Sutton S, Tueting P, Zubin J and John E R 1967 Information delivery and the sensory evoked potential *Science* **155** 1436–9
[75] Yamada T, Rodnitzky R L, Kameyama S, Matsuoka H and Kimura J 1991 Alteration of SEP topography in Huntington's patients and their relatives at risk *Electroencephalogr. Clin. Neurophysiol.* **80** 251–61
[76] Huang Y, Dmochowski J P, Su Y, Datta A, Rorden C and Parra L C 2013 Automated MRI segmentation for individualized modeling of current flow in the human head *J. Neural Eng.* **10** 066004
[77] Towle V L *et al* 1993 The spatial location of EEG electrodes: locating the best-fitting sphere relative to cortical anatomy *Electroencephalogr. Clin. Neurophysiol.* **86** 1–6
[78] Eshel Y and Abboud S 1997 Correlation between source asymmetry and scalp potential asymmetry in a prolate spheroid model of the head *Comput. Biol. Med.* **27** 87–96
[79] Nathan S S, Sinha S R, Gordon B, Lesser R P and Thakor N V 1993 Determination of current density distributions generated by electrical stimulation of the human cerebral cortex *Electroencephalogr. Clin. Neurophysiol.* **86** 183–92
[80] Smith W E 1992 Estimation of the spatio-temporal correlations of biological electrical sources from their magnetic fields *IEEE Trans. Bio-Medical Eng.* **39** 997–1004
[81] Stinstra J G and Peters M J 1998 The volume conductor may act as a temporal filter on the ECG and EEG *Med. Biol. Eng. Comput.* **36** 711–6
[82] Liu Q, Balsters J H, Baechinger M, van der Groen O, Wenderoth N and Mantini D 2015 Estimating a neutral reference for electroencephalographic recordings: the importance of using a high-density montage and a realistic head model *J. Neural Eng.* **12** 056012
[83] Michel C M, Murray M M, Lantz G, Gonzalez S, Spinelli L and Grave de Peralta R 2004 EEG source imaging *Clin. Neurophysiology: Official J. Int. Fed. Clin. Neurophysiology* **115** 2195–222
[84] Song J *et al* 2015 EEG source localization: sensor density and head surface coverage *J. Neurosci. Methods* **256** 9–21
[85] Cancelli A *et al* 2015 Transcranial direct current stimulation: personalizing the neuromodulation *Conf. Proc.: Annual Int. Conf. of the IEEE Engineering in Medicine and Biology Society* vol 2015 pp 234–7
[86] De Ridder D and Vanneste S 2012 EEG driven tDCS versus bifrontal tDCS for tinnitus *Frontiers Psychiatry* **3** 84
[87] Del Felice A, Magalini A and Masiero S 2015 Slow-oscillatory transcranial direct current stimulation modulates memory in temporal lobe epilepsy by altering sleep spindle generators: a possible rehabilitation tool *Brain Stimulation* **8** 567–73
[88] Dannhauer M, Brooks D, Tucker D and MacLeod R 2012 A pipeline for the simulation of transcranial direct current stimulation for realistic human head models using SCIRun/BioMesh3D *Conf. Proc.: Annual Int. Conf. of the IEEE Engineering in Medicine and Biology Society* vol 2012 5486–9
[89] Gillick B T, Kirton A, Carmel J B, Minhas P and Bikson M 2014 Pediatric stroke and transcranial direct current stimulation: methods for rational individualized dose optimization *Frontiers Hum. Neurosci.* **8** 739
[90] Huang Y and Parra L C 2015 Fully automated whole-head segmentation with improved smoothness and continuity, with theory reviewed *PloS One* **10** e0125477
[91] Edwards D, Cortes M, Datta A, Minhas P, Wassermann E M and Bikson M 2013 Physiological and modeling evidence for focal transcranial electrical brain stimulation in humans: a basis for high-definition tDCS *NeuroImage* **74** 266–75
[92] Haufe S, Huang Y and Parra L C 2015 A highly detailed FEM volume conductor model based on the ICBM152 average head template for EEG source imaging and TCS targeting *Conf. Proc.: Annual Int. Conf. of the IEEE Engineering in Medicine and Biology Society* vol 2015 pp 5744–7
[93] Schmidt C, Wagner S, Burger M, Rienen U and Wolters C H 2015 Impact of uncertain head tissue conductivity in the optimization of transcranial direct current stimulation for an auditory target *J. Neural Eng.* **12** 046028
[94] Huang Y, Parra L C and Haufe S 2015 The New York Head-A precise standardized volume conductor model for EEG source localization and tES targeting *NeuroImage* **15** S1053–8119
[95] Fiederer L D *et al* 2016 The role of blood vessels in high-resolution volume conductor head modeling of EEG *NeuroImage* **128** 193–208
[96] Muthalib M, Besson P, Rothwell J, Ward T and Perrey S 2016 Effects of anodal high-definition transcranial direct current stimulation on bilateral sensorimotor cortex activation during sequential finger movements: an fNIRS study *Adv. Exp. Med. Biol.* **876** 351–9
[97] Caparelli-Daquer E M, Valente A F, Nigri F, Edwards D J and Medeiros A H 2016 A halo-shaped electrode holder system for HD-tDCS is a practical and flexible alternative to the EEG Cap 4 × 1-ring montage *Brain Stimulation* **9** 153–5
[98] Flood A, Waddington G and Cathcart S 2016 High-definition transcranial direct current stimulation enhances conditioned pain modulation in healthy volunteers: a randomised trial *J. Pain: Official J. Am. Pain Soc.* **17** 600–5
[99] Villamar M F, Volz M S, Bikson M, Datta A, Dasilva A F and Fregni F 2013 Technique and considerations in the use of 4 × 1 ring high-definition transcranial direct current stimulation (HD-tDCS) *J. Visualized Exp.: JoVE* **77** e50309
[100] Loo C K, Martin D M, Alonzo A, Gandevia S, Mitchell P B and Sachdev P 2011 Avoiding skin burns with transcranial direct current stimulation: preliminary considerations *Int. J. Neuropsychopharmacology/Official Sci. J. Collegium Internationale Neuropsychopharmacologicum* **14** 425–6
[101] DaSilva A F, Truong D Q, DosSantos M F, Toback R L, Datta A and Bikson M 2015 State-of-art neuroanatomical target analysis of high-definition and conventional tDCS montages used for migraine and pain control *Frontiers Neuroanatomy* **9** 89
[102] Antal A, Boros K, Poreisz C, Chaieb L, Terney D and Paulus W 2008 Comparatively weak after-effects of transcranial alternating current stimulation (tACS) on cortical excitability in humans *Brain Stimulation* **1** 97–105
[103] Fröhlich F 2015 Experiments and models of cortical oscillations as a target for noninvasive brain stimulation *Prog. Brain Res.* **222** 41–73
[104] Pollok B, Boysen A C and Krause V 2015 The effect of transcranial alternating current stimulation (tACS) at alpha and beta frequency on motor learning *Behav. Brain Res.* **293** 234–40
[105] Witkowski M *et al* 2015 Mapping entrained brain oscillations during transcranial alternating current stimulation (tACS) *NeuroImage* **15** S1053–8119
[106] Helfrich R F, Schneider T R, Rach S, Trautmann-Lengsfeld S A, Engel A K and Herrmann C S 2014 Entrainment of brain oscillations by transcranial alternating current stimulation *Curr. Biol.: CB* **24** 333–9

[107] Herrmann C S, Rach S, Neuling T and Struber D 2013 Transcranial alternating current stimulation: a review of the underlying mechanisms and modulation of cognitive processes *Frontiers Hum. Neurosci.* **7** 279
[108] Delorme A and Makeig S 2004 EEGLAB: an open source toolbox for analysis of single-trial EEG dynamics including independent component analysis *J. Neurosci. Methods* **134** 9–21
[109] Barbati G, Porcaro C, Zappasodi F, Rossini P M and Tecchio F 2004 Optimization of an independent component analysis approach for artifact identification and removal in magnetoencephalographic signals *Clin. Neurophysiology: Official J. Int. Fed. Clin. Neurophysiology* **115** 1220–32
[110] Porcaro C, Medaglia M T and Krott A 2015 Removing speech artifacts from electroencephalographic recordings during overt picture naming *NeuroImage* **105** 171–80
[111] Bidelman G M 2015 Multichannel recordings of the human brainstem frequency-following response: scalp topography, source generators, and distinctions from the transient ABR *Hear. Res.* **323** 68–80
[112] Jeran J, Koritnik B, Zidar I, Belic A and Zidar J 2013 Sniffing-related motor cortical potential: topography and possible generators *Respiratory Physiol. Neurobiology* **185** 249–56
[113] Feng W, Stormer V S, Martinez A, McDonald J J and Hillyard S A 2014 Sounds activate visual cortex and improve visual discrimination *J. Neurosci.: Official J. Soc. Neurosci.* **34** 9817–24
[114] Tenke C E and Kayser J 2015 Surface laplacians (SL) and phase properties of EEG rhythms: simulated generators in a volume-conduction model *Int. J. Psychophysiology: Official J. Int. Organ. Psychophysiology* **97** 285–98
[115] Wang M, Yang P, Zhao Q J, Wang M, Jin Z and Li L 2016 Differential preparation intervals modulate repetition processes in task switching: an ERP study *Frontiers Hum. Neurosci.* **10** 57
[116] Kilicarslan A, Grossman R G and Contreras-Vidal J L 2016 A robust adaptive denoising framework for real-time artifact removal in scalp EEG measurements *J. Neural Eng.* **13** 026013
[117] Valderrama J T, de la Torre A, Medina C, Segura J C and Thornton A R 2016 Selective processing of auditory evoked responses with iterative-randomized stimulation and averaging: a strategy for evaluating the time-invariant assumption *Hear. Res.* **333** 66–76
[118] Truong D Q, Magerowski G, Blackburn G L, Bikson M and Alonso-Alonso M 2013 Computational modeling of transcranial direct current stimulation (tDCS) in obesity: impact of head fat and dose guidelines *NeuroImage Clin.* **2** 759–66
[119] Phillips C, Rugg M D and Friston K J 2002 Anatomically informed basis functions for EEG source localization: combining functional and anatomical constraints *NeuroImage* **16** 678–95
[120] Anemuller J, Sejnowski T J and Makeig S 2003 Complex independent component analysis of frequency-domain electroencephalographic data *Neural Netw.: Official J. Int. Neural Netw. Soc.* **16** 1311–23
[121] Porcaro C, Medaglia M T, Thai N J, Seri S, Rotshtein P and Tecchio F 2014 Contradictory reasoning network: an EEG and FMRI study *PloS One* **9** e92835
[122] von Ellenrieder N *et al* 2016 Detection and magnetic source imaging of fast oscillations (40–160 Hz) recorded with magnetoencephalography in focal epilepsy patients *Brain Topography* **29** 218–31
[123] Pizzagalli D A, Sherwood R J, Henriques J B and Davidson R J 2005 Frontal brain asymmetry and reward responsiveness: a source-localization study *Psychological Sci.* **16** 805–13
[124] Van Veen B D, van Drongelen W, Yuchtman M and Suzuki A 1997 Localization of brain electrical activity via linearly constrained minimum variance spatial filtering *IEEE Trans. Bio-Medical Eng.* **44** 867–80
[125] Pascual-Marqui R D, Michel C M and Lehmann D 1994 Low resolution electromagnetic tomography: a new method for localizing electrical activity in the brain *Int. J. Psychophysiology: Official J. Int. Organ. Psychophysiology* **18** 49–65
[126] Melgari J M *et al* 2013 Movement-induced uncoupling of primary sensory and motor areas in focal task-specific hand dystonia *Neuroscience* **250** 434–45
[127] Porcaro C *et al* 2013 Multiple frequency functional connectivity in the hand somatosensory network: an EEG study *Clin. Neurophysiology: Official J. Int. Fed. Clin. Neurophysiology* **124** 1216–24
[128] Kohler P J, Clarke A, Yakovleva A, Liu Y and Norcia A M 2016 Representation of maximally regular textures in human visual cortex *J. Neurosci.: Official J. Soc. Neurosci.* **36** 714–29
[129] Grech R *et al* 2008 Review on solving the inverse problem in EEG source analysis *J. Neuroengineering Rehab.* **5** 25
[130] Pascarella A, Todaro C, Clerc M, Serre T and Piana M 2016 Source modeling of ElectroCorticoGraphy (ECoG) data: stability analysis and spatial filtering *J. Neurosci. Methods* **263** 134–44
[131] Mayhew S D, Ostwald D, Porcaro C and Bagshaw A P 2013 Spontaneous EEG alpha oscillation interacts with positive and negative BOLD responses in the visual-auditory cortices and default-mode network *NeuroImage.* **76** 362–72
[132] Levine S P *et al* 2000 A direct brain interface based on event-related potentials *IEEE Trans. Rehab. Eng.: Publ. IEEE Eng. Med. Biol. Soc.* **8** 180–5
[133] Bandarabadi M, Teixeira C A, Rasekhi J and Dourado A 2015 Epileptic seizure prediction using relative spectral power features *Clin. Neurophysiology: Official J. Int. Fed. Clin. Neurophysiology* **126** 237–48
[134] Yu T, Yu Z, Gu Z and Li Y 2015 Grouped automatic relevance determination and its application in channel selection for P300 BCIs *IEEE Trans. Neural Syst. Rehab. Eng.: Publ. IEEE Eng. Med. Biol. Soc.* **23** 1068–77
[135] Garrett D, Peterson D A, Anderson C W and Thaut M H 2003 Comparison of linear, nonlinear, and feature selection methods for EEG signal classification *IEEE Trans. Neural Syst. Rehab Eng.: Publ. IEEE Eng. Med. Biol. Soc.* **11** 141–4
[136] Wang S, Li Y, Wen P and Lai D 2016 Data selection in EEG signals classification *Australas. Phys. Eng. Sci. Med.* /Supported by the Australasian College of Physical Scientists in Medicine and the Australasian Association of Physical Sciences in Medicine **39** 157–65
[137] Faul S D 2010 Dynamic channel selection to reduce computational burden in seizure detection *Conf. Proc.: Annual Int. Conf. of the IEEE Engineering in Medicine and Biology Society* vol 2010 pp 6365–8
[138] Cichocki A and Sanei S 2007 EEG/MEG signal processing *Comput. Intell. Neurosci.* **97026**
[139] Todd M M 1998 EEGs, EEG processing, and the bispectral index *Anesthesiology* **89** 815–7